

# Paramagnon heat capacity and anomalous thermopower in anisotropic magnetic systems: Understanding interlayer spin correlations in a magnetically disordered phase

Fatemeh Heydarinasab<sup>1,\*</sup>, Morteza Jazandari<sup>2,\*</sup>, Md Mobarak Hossain Polash,<sup>3,4</sup> Jahanfar Abouie<sup>2,†</sup> and Daryoosh Vashae<sup>3,4,‡</sup>

<sup>1</sup>*Department of Physics, Faculty of Science, University of Sistan and Baluchestan, Zahedan 98167-45845, Iran*

<sup>2</sup>*Department of Physics, Institute for Advanced Studies in Basic Sciences (IASBS), Zanjan 45137-66731, Iran*

<sup>3</sup>*Department of Materials Science and Engineering, North Carolina State University, Raleigh, North Carolina 27606, USA*

<sup>4</sup>*Department of Electrical and Computer Engineering, North Carolina State University, Raleigh, North Carolina 27606, USA*



(Received 5 September 2023; revised 29 November 2023; accepted 14 December 2023; published 14 February 2024)

The interplay between entropy transport and charge carriers–paramagnon interaction in the Onsager linear system has been a subject of debate due to the limited theoretical and experimental understanding of paramagnon heat capacity. In this study, we investigate this interplay in an anisotropic layered magnetic system using cluster mean-field theory with spin quantum correlations. By examining spin correlation functions between different spins with various types of clustering, we derive the spin correlation function as a function of distance and temperature for the interlayer clusters both below and above the magnetic order phase transition. Our analysis reveals that paramagnons characterized by pronounced spin correlations among interlayer nearest-neighbor spins exhibit a nonzero heat capacity, providing valuable insights into the dynamics of entropy transport. The findings align with experimental observations, lending strong support to the validity of the paramagnon-drag thermopower concept. This study sheds light on the intricate dynamics and thermodynamic properties of paramagnons, advancing our understanding of entropy transport in complex systems.

DOI: [10.1103/PhysRevB.109.054418](https://doi.org/10.1103/PhysRevB.109.054418)

## I. INTRODUCTION

Spin-driven thermoelectrics has emerged as a promising avenue to enhance the performance of thermoelectric materials. Traditional approaches primarily focused on electron and phonon transport properties, but their limitations have sparked a growing interest in exploring spin-based materials [1–4]. In particular, the paramagnon-electron drag (PED) thermopower has emerged as a compelling phenomenon, exhibiting continuous enhancement in the paramagnetic phase and offering the potential for high-performance thermoelectric devices [5–7].

Paramagnons, arising from thermal fluctuations in the disordered phase, can exhibit magnonlike behavior when specific conditions are met [5,6,8–11]. Experimental evidence, including nonzero drag thermopower and extended magnon lifetime, supports the concept [5,6]. The effect has led to achieving a practical  $zT > 1$  at  $T > 800$  K in MnTe [6]. Furthermore, the magnon-electron drag phenomenon is linked to the spin-Seebeck effect in paramagnetic materials [12–14], while thermal fluctuations enhance  $zT$  in CoSb<sub>3</sub> superparamagnets [15]. *Ab initio* calculations have explored spin correlation functions in the paramagnetic regime, providing a real-space perspective [16]. These findings emphasize the potential

of paramagnon-based processes in enhancing thermoelectric performance.

Despite the prospects of PED, the underlying origin of the excess spin-contributed thermopower in paramagnetic materials remains a subject of debate [5,17]. It has been hypothesized that paramagnons, resembling magnons to itinerant carriers, give rise to paramagnon-drag thermopower due to their longer lifetime and larger spatial correlation length compared to free carrier's characteristic length scales [6]. However, a comprehensive understanding of the nature and thermodynamic properties of paramagnons is still lacking. Establishing the paramagnon heat capacity as an essential component for validating the PED thermopower concept has been recognized [5,17,18].

The heat capacity, which quantifies the entropy change with temperature, and the thermopower, which measures the entropy transported by charge carriers, suggest that paramagnons could contribute to heat capacity through momentum transfer, leading to PED thermopower [19,20]. While experimental observations have shown nonzero magnetic heat capacities above the phase transition temperatures for various magnetic materials [6,7,21,22], the role of paramagnons in contributing to paramagnetic heat capacity has often been overlooked. Multiple factors, including changes in free energy associated with magnetic ordering-disordering, spin fluctuations, Schottky contributions, and other second-order phase changes, can contribute to nonzero magnetic heat capacities above the transition temperature [22–26]. However, a lack of theoretical understanding of paramagnon heat capacity has hindered a comprehensive assessment of their entropy

\*These authors contributed equally to this work.

†Corresponding author: [jahan@iasbs.ac.ir](mailto:jahan@iasbs.ac.ir)

‡Corresponding author: [dvashae@ncsu.edu](mailto:dvashae@ncsu.edu)

contribution. In this study, we aim to bridge this gap by conducting a detailed theoretical investigation to understand and quantify the contribution of paramagnons to heat capacity, which can provide insights into the presence of different entropy carriers in the host materials [22,27–29].

Moreover, it is crucial to clarify the connection between magnons and paramagnons in the context of this study. While both magnons and paramagnons represent collective spin excitations in magnetic materials, they play different roles depending on the material's magnetic phase. Magnons typically emerge in the ordered (magnetic) phase and are collective quantum excitations arising from the alignment of neighboring atomic spins. They contribute to various thermodynamic properties of the material in the ordered phase. In contrast, paramagnons manifest in the paramagnetic phase, which occurs at high temperatures when thermal energy disrupts the alignment of atomic spins, resulting in an average nonmagnetic state. Paramagnons represent collective spin fluctuations that persist in this disordered phase and contribute to the heat capacity of the material. Understanding this connection between magnons and paramagnons is essential for unraveling the intricacies of spin-driven thermoelectricity. We focus on paramagnons and their behavior in the paramagnetic phase, particularly how spin correlations among interlayer nearest-neighbor spins influence the specific heat to gain insights into the intricate dynamics of paramagnons and enhance our understanding of entropy transport in complex systems.

To explore the paramagnon heat capacity in disordered spin clusters, we employ a cluster mean-field (CMF) theory, which incorporates thermal fluctuations essential for magnon generation [5–7]. Compared to other techniques like quantum Monte Carlo simulations, CMF offers distinct advantages, enabling the examination of short-range orders in different directions and the determination of specific contributions of paramagnon types to the specific heat and thermopower above the critical temperature. In contrast to Monte Carlo simulations, which provide an overall behavior of the specific heat, CMF provides valuable insights into the role of paramagnons in the thermodynamic properties of the system.

We compare the CMF theory with other established approaches commonly used in the study of magnetic materials, such as mean-field (MF) and spin-wave (SW) theories [20,30]. While SW and MF theories primarily focus on long-range order parameters and may not fully account for short-range correlations, CMF theory offers a more comprehensive approach. CMF theory includes the exact shapes of spin-spin interactions within clusters, providing a level of detail that is typically overlooked in SW and MF methods. This inclusion of short-range correlations through CMF is crucial for shedding light on the paramagnon concept, especially at temperatures above  $T_N$ . These short-range correlations are a defining characteristic of paramagnons and play a significant role in understanding the system's behavior in the paramagnetic phase. By considering different types of clusters, the CMF theory allows us to investigate the influence of short-range correlations on paramagnon heat capacity and gain a comprehensive understanding of the spin dynamics in paramagnon-electron drag phenomena. To validate our calculations, we compare the derived paramagnon heat capacity with experimental results obtained from MnTe, a

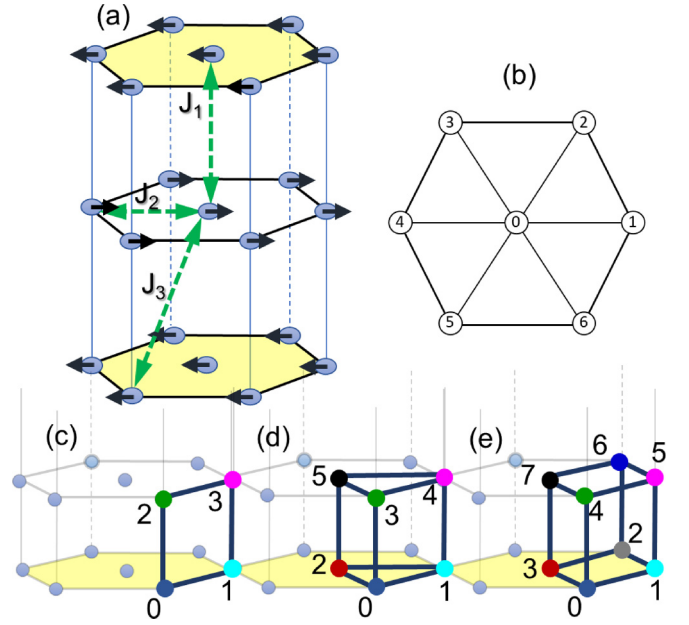


FIG. 1. (a) A three-dimensional layered spin system with AFM interlayer interactions  $J_1$  and  $J_3$ , and intralayer FM interaction  $J_2$ . Arrows show the spin order in the AFM phase below a Néel temperature. (b) MF sublattice structure of the spin Hamiltonian in every layer, which respects the symmetry of the lattice. (c), (d) and (e) are four-, six-, and eight-site clusters used in CMF4, CMF6, and CMF8 theory.

material system known for its relevance in studying the magnon/paramagnon-drag effect [5,6,31].

## II. METHODS

We consider a three-dimensional layered spin-1 system described by the following Hamiltonian:

$$H = J_1 \sum_{\ell,j} \vec{S}_{\ell,j} \cdot \vec{S}_{\ell+1,j} + \sum_{\ell,(i,j)} (J_2 \vec{S}_{\ell,i} \cdot \vec{S}_{\ell,j} + J_3 \vec{S}_{\ell,i} \cdot \vec{S}_{\ell+1,j}), \quad (1)$$

where  $J_1 > 0$  is the interlayer nearest-neighbor (NN) antiferromagnetic (AFM) interaction,  $J_2 < 0$  is the intralayer NN ferromagnetic (FM) interaction, and  $J_3 > 0$  is the diagonal interlayer AFM interaction [Fig. 1(a)]. Here, the summations on  $\ell$  run over different layers, and the summations on  $(i, j)$  run over different NN sites. To compare with experimental data, we choose MnTe with  $J_1 = 21.5$  K,  $J_2 = -0.67$  K, and  $J_3 = 2.81$  K [5,32]. The larger value of  $J_1$  enables us to categorize the system into two types of layers with different magnetizations ( $\vec{m}_A$  and  $\vec{m}_B$ ), which we consider in both the MF and the CMF calculations. Utilizing these theories, we calculate the staggered magnetization and specific heat by  $C_V = \partial \langle H \rangle / \partial T$ , where  $\langle H \rangle$  is the internal energy and  $T$  denotes temperature [20].

In the MF approximation, the spin-spin interactions are typically replaced by the average of the individual spin components ( $\vec{S}_i$  or  $\vec{S}_j$ ). This is represented mathematically as  $\vec{S}_i \cdot \vec{S}_j = \vec{S}_i \langle \vec{S}_j \rangle + \vec{S}_j \langle \vec{S}_i \rangle - \langle \vec{S}_i \rangle \langle \vec{S}_j \rangle$ . In our study, we adopt a general approach and consider different sublattices in each layer [as shown in Fig. 1(b)]. This allows us to explore a

wide range of possibilities and investigate the effects of varying sublattices on the system's behavior. Therefore, the spin Hamiltonian in the MF approximation is written as

$$\frac{H_{MF}}{N} = 2J_1 \sum_{j=0}^6 (\vec{S}_{0,j} \cdot \vec{m}_{1,j} + \vec{S}_{1,j} \cdot \vec{m}_{0,j}) + \sum_{i,j=0,i \neq j}^6 \left( J_2 (\vec{S}_{0,i} \cdot \vec{m}_{0,j} + \vec{S}_{1,i} \cdot \vec{m}_{1,j}) + 2J_3 (\vec{S}_{0,i} \cdot \vec{m}_{1,j} + \vec{S}_{1,i} \cdot \vec{m}_{0,j}) \right), \quad (2)$$

where  $\vec{m}_{\ell,j} = \langle \vec{S}_{\ell,j} \rangle_{MF}$  with  $\ell = 0, 1$  the MF magnetization vector in layer  $\ell$  at site  $j$ .  $N$  is the number of unit cells, wherein each unit cell consists of two layers with seven spins denoted by labels ranging from 0 to 6, as shown in Fig. 1(b), and the summations on  $i$  and  $j$  run over different sublattices. The self-consistent solution of Eq. (2) yields the MF magnetizations and energy of the system, which, in turn, enables the calculation of the specific heat.

The MF method neglects spin-spin correlations, leading to a lack of finite specific heat in disordered regions. Thus, incorporating spin-spin correlations is crucial for capturing finite specific heat in disordered regions. The Bethe method, considering nearest-neighbor interactions, reveals short-range orders and nonzero specific heat even above the transition temperature, resembling real physical systems [33]. Further modifications, such as the Onsager solution, improve consistency with experiments [33,34]. However, applying these methods to our three-dimensional spin system is challenging. To account for more correlations, we employ a CMF theory, treating clusters of multiple sites instead of the single-site approximation [35–37]. CMF theory effectively incorporates quantum fluctuations and spin correlations by considering interactions within the clusters and treating spins outside the clusters as effective fields [38–40]. Hence, the corresponding CMF Hamiltonian can be defined as [35–37]

$$H_{CMF} = \sum_c (H_c + h_{\text{eff}}), \quad (3)$$

where  $H_c$  and  $h_{\text{eff}}$  contain the interactions within and between the clusters, respectively. Here, the summation on  $c$  runs over different clusters. For the case of a cluster with four sites, the Hamiltonian, labeled as CMF4, is given by  $H_{CMF4} = \sum_c (H_{c-4} + h_{\text{eff}-4})$ , with

$$H_{c-4} = J_1 (\vec{S}_0 \cdot \vec{S}_2 + \vec{S}_1 \cdot \vec{S}_3) + J_2 (\vec{S}_0 \cdot \vec{S}_1 + \vec{S}_2 \cdot \vec{S}_3) + J_3 (\vec{S}_0 \cdot \vec{S}_3 + \vec{S}_1 \cdot \vec{S}_2),$$

$$h_{\text{eff}-4} = J_1 (\vec{S}_0 \cdot \vec{m}_2 + \vec{S}_1 \cdot \vec{m}_3 + \vec{S}_2 \cdot \vec{m}_0 + \vec{S}_3 \cdot \vec{m}_1) + J_2 \{ \vec{S}_0 \cdot (2\vec{m}_0 + 3\vec{m}_1) + \vec{S}_1 \cdot (2\vec{m}_1 + 3\vec{m}_0) + \vec{S}_2 \cdot (2\vec{m}_2 + 3\vec{m}_3) + \vec{S}_3 \cdot (2\vec{m}_3 + 3\vec{m}_2) \} + J_3 \{ \vec{S}_0 \cdot (4\vec{m}_2 + 7\vec{m}_3) + \vec{S}_1 \cdot (4\vec{m}_3 + 7\vec{m}_2) + \vec{S}_2 \cdot (4\vec{m}_0 + 7\vec{m}_1) + \vec{S}_3 \cdot (4\vec{m}_1 + 7\vec{m}_0) \},$$

where four-site clusters are illustrated in Fig. 1(c). Here,  $\vec{m}_i$  is the magnetization vector at the  $i$ th sublattice. Like the MF, the self-consistent solution of the CMF Hamiltonian provides the CMF energy and hence the specific heat.

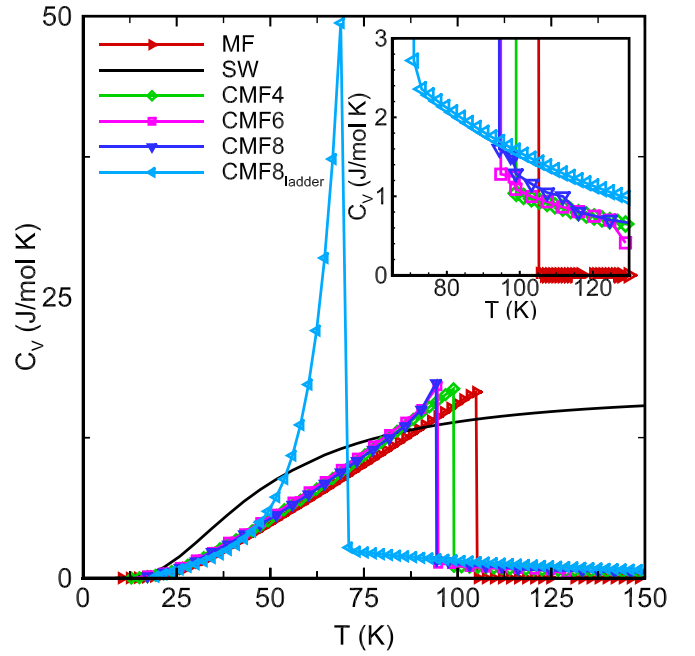


FIG. 2. Specific heat estimation for the  $S = 1$  spin system using MF, SW, CMF4, CMF6, and CMF8 methods. Cluster shapes for CMF4, CMF6, and CMF8 are shown in Fig. 1. CMF8<sub>ladder</sub> is the CMF8 results for specific heat with ladder-type configurations presented in the inset of Fig. 3(b). Calculated data is represented by symbols, and solid lines serve as visual guides. In the inset, the specific heat for temperatures above  $T_N$  is highlighted.

Incorporating the FM  $J_2$  interaction, we construct cluster configurations that consider the influence of  $J_1$  and  $J_3$  interactions [Figs. 1(c)–1(e)]. The corresponding CMF Hamiltonian is defined for each configuration. For an  $n$ -site cluster with  $n = 4, 6, 8$ , the Hamiltonian, denoted as CMFn, is articulated in Eq. (3), with  $H_c = H_{c-n}$  and  $h_{\text{eff}} = h_{\text{eff}-n}$  (see the Appendix). Thermal fluctuations are accounted for in MF, SW, and CMF theories, resulting in a reduction of the order parameter until the transition temperature  $T_N$ , where it eventually vanishes. The CMF theory predicts a lower  $T_N$  compared to the MF approximation due to the inclusion of spin correlations (see the Appendix).

### III. RESULTS

The estimated specific heat using the MF approximation, SW theory, and CMF method is illustrated in Fig. 2. According to the MF approximation, the  $C_V$  grows up to  $T_N$ , drops sharply at  $T_N$ , and vanishes at higher temperatures. Compared to the other results, the MF method overestimated the transition temperature. Conversely, the SW method, despite partially including quantum fluctuations, displays a deviation in the specific heat trend over a significant temperature range. Although it provides accurate estimates at low temperatures, it overestimates and saturates as the temperature increases.

At this point, it is important to clarify the transition between magnons and paramagnons in the context of specific heat behavior. At low temperatures, the system is primarily governed by long-wavelength spin excitations known as

magnons, and the linear SW theory excels in capturing their behavior, especially when  $C_V$  is proportional to  $T^3$  ( $T^{3/2}$ ) near the antiferromagnetic (ferromagnetic) ground state [41]. However, as temperatures increase, the system transitions into the paramagnetic phase ( $T > T_N$ ), characterized by disrupted long-range magnetic order and the emergence of short-range correlations known as paramagnons. Unlike SW theory, CMF theory accurately accounts for these short-range correlations within clusters, offering a more accurate representation of thermodynamic properties in the paramagnetic regime. This distinction underscores the importance of short-range correlations and explains the failure of SW theory in estimating specific heat across temperature ranges. Our results, detailed in Fig. 2, consistently reveal deviations between SW and CMF models even well below  $T_N$ , highlighting the significance of thermal fluctuation of magnetization in governing specific heat at elevated temperatures.

Our specific heat results from the CMF(4,6,8) theory (Fig. 2) show a similar trend to the MF method up to the transition temperature. However, unlike the MF approximation, our CMF theory predicts a finite value for the specific heat in the disordered paramagnetic phase. Notably, the CMF theory provides a better estimation of specific heat in both ordered and disordered phases. Estimating nonzero specific heat in disordered phases from the correlations of the spins inside clusters is a successful demonstration of paramagnon contributions. The results can be an essential argument for the existence of the PED thermopower.

As depicted in Fig. 2, considering larger cluster sizes to include more correlations improves the behavior of  $C_V$  in the disordered phase, attributed to higher energy fluctuations. Due to the anisotropic nature of our spin system, similar to the ordered phase where two layers host two types of magnons with the same energy dispersion, the disordered phase can exhibit two types of paramagnons. One type corresponds to collective excitations of spins within cuboid-shaped clusters, as illustrated in Fig. 1(e). These paramagnons disperse across the triangular layers and contribute to the system's internal energy, resulting in a nonzero specific heat above the Néel temperature. The other type corresponds to collective excitations of spins within ladder-shaped clusters, aligned with the system's dominant exchange interaction ( $J_1$ ), as shown in the inset of Fig. 3(b). Considering the influence of these paramagnons can lead to intriguing outcomes and provide further insight into the system's behavior.

The strong spin fluctuations in the system are best examined by considering vertical clusters, and including more correlations in the system enhances the observation of the specific heat behavior above the critical temperature (see Fig. 2, CMF8<sub>ladder</sub>). Consequently, incrementally increasing the cluster sizes and configurations enhances the paramagnetic specific heat trend towards the transition temperature.

We also estimate the spin correlation functions between NN and next-nearest-neighbor (NNN) spins along the  $J_1$  direction [Fig. 3(a)], obtained by CMF8 with a ladder [Fig. 3(b), inset] type of clustering (see the Appendix for the exact definition of this type of clustering). Here, the spin-spin correlation is defined by

$$\langle \vec{S}_i \cdot \vec{S}_j \rangle_c = \langle \vec{S}_i \cdot \vec{S}_j \rangle - \langle \vec{S}_i \rangle \langle \vec{S}_j \rangle. \quad (4)$$

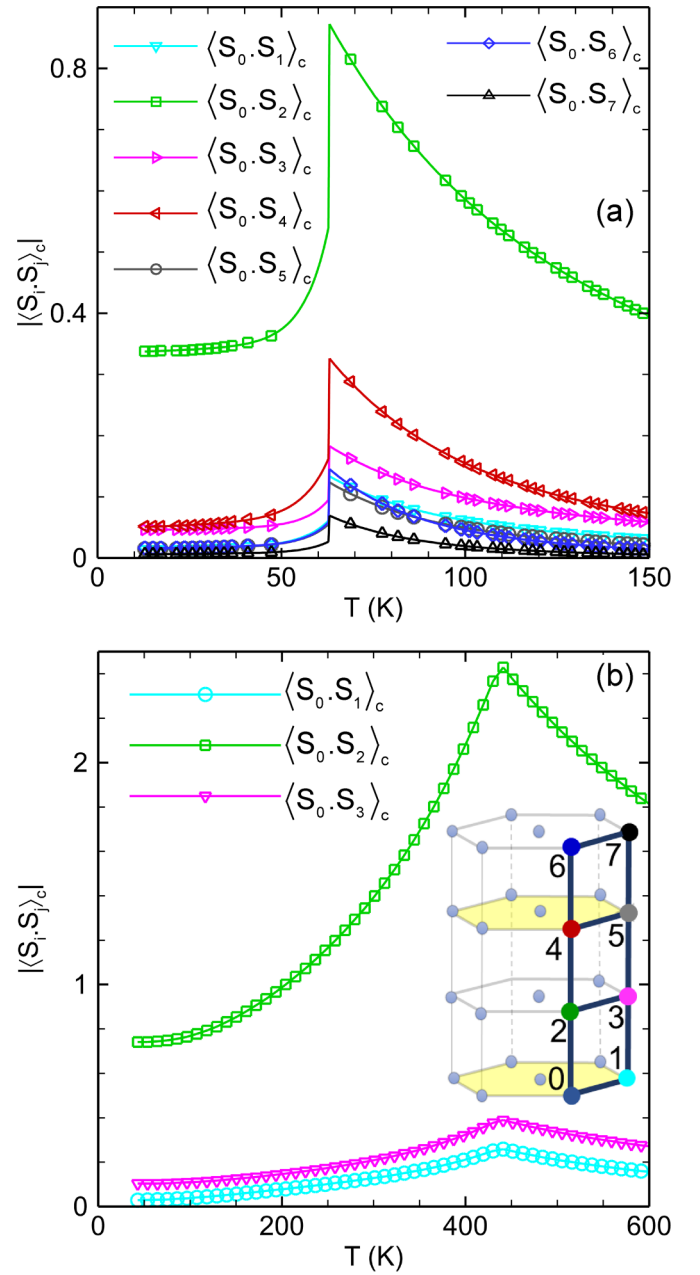


FIG. 3. (a) Spin correlation functions between different spins in the spin-1 system as a function of temperature obtained using CMF8<sub>ladder</sub> with various types of clustering, as shown in the inset (b). The symbols represent the calculated results, while solid lines serve as visual guides. (b) Spin correlation functions between different spins in the  $S = 5/2$  system such as MnTe, obtained using CMF4. Due to computational limitations, the CMF(6,8) theories are not applicable to the spin-5/2 system, and the correlation function between the spins in the NNN layers are not reported for the CMF(6,8).

Intriguingly, spin-spin correlations along the  $J_1$  direction involving further neighbors (e.g.,  $\langle \vec{S}_0 \cdot \vec{S}_4 \rangle_c$ ) prove to be stronger than those with direct  $J_2$  and  $J_3$  interactions (e.g.,  $\langle \vec{S}_0 \cdot \vec{S}_1 \rangle_c$  and  $\langle \vec{S}_0 \cdot \vec{S}_3 \rangle_c$ ). These pronounced interlayer correlations along  $J_1$  improve the specific heat trend in the disordered phase, as evident in the CMF8<sub>ladder</sub> plot in Fig. 2.

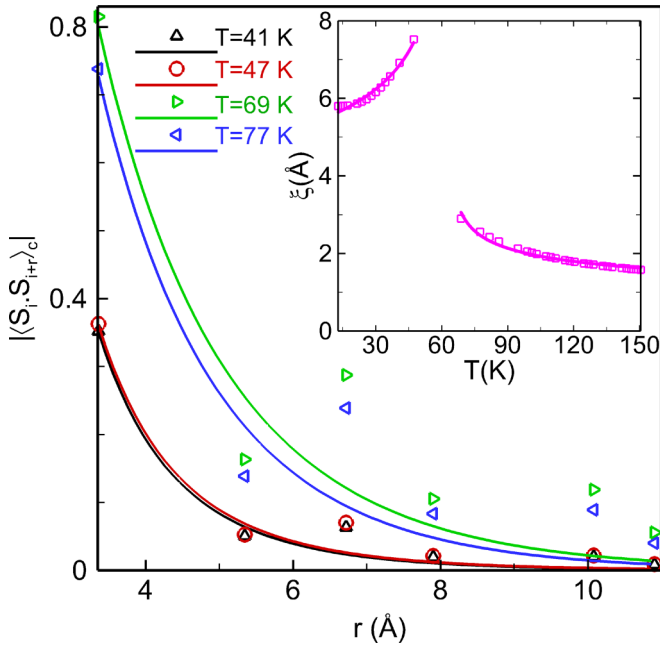


FIG. 4. The absolute value of the spin correlation function as a function of distance  $r$  for various temperatures in the spin-1 system on the MnTe lattice, obtained using the CMF8 approach with ladder-type clustering. The inset depicts the correlation length ( $\xi$ ) versus temperature for the spin-1 system with eight-site clusters and ladder-type configuration, where the symbols represent the calculated results and the solid lines represent the fitted results.

Given this high degree of correlation, selecting clusters along the vertical or  $J_1$  direction leads to a pronounced peak, outperforming other clusters. This observation suggests the emergence of robust spin excitations, potentially manifesting as paramagnons with the potential for high PED.

As previously discussed, the inclusion of spin correlations through CMF theory introduces modifications to the specific heat's behavior. Notably, fluctuations around the mean-field solution play a significant role in the free energy and specific heat of the system. To illustrate, when these fluctuations exhibit Gaussian correlations, their contribution to the specific heat ( $C_F$ ) can be described by the following expression [42]:

$$C_F \sim \int d^3k (k^2 + \xi^{-2})^{-2}, \quad (5)$$

Here,  $\xi$  represents the correlation length. By rescaling  $k$  with  $\xi^{-1}$  and performing this integral, we find that the specific heat  $C_F$  is proportional to  $\xi$ . Consequently, investigating how the correlation length varies with temperature becomes a valuable approach for understanding specific heat behavior.

To investigate the temperature dependence of the correlation length and its critical exponents, we have created plots in Fig. 4. These plots depict the correlation function against the distance “ $r$ ” for various temperatures: 41 and 47 K for temperatures below  $T_N$ , and 69 and 77 K for temperatures above  $T_N$ . We performed fittings using the following well-established

function [33]:

$$\begin{aligned} \langle \vec{S}_i \cdot \vec{S}_{i+r} \rangle_c &= A_- \frac{e^{-2r/\xi}}{(r/\xi)^2}, & T < T_N \\ &= A_+ \frac{e^{-r/\xi}}{(r/\xi)^{1/2}}, & T > T_N. \end{aligned} \quad (6)$$

In these equations, the coefficients  $A_{\pm}$  vary depending on the temperature. The critical exponents of the correlation length are determined through the fit of the correlation length with temperature using the following equations [42]:

$$\begin{aligned} \xi &= B_- \frac{1}{(1 - T/T_N)^{\nu_-}}, & T < T_N \\ &= B_+ \frac{1}{(T/T_N - 1)^{\nu_+}}, & T > T_N. \end{aligned} \quad (7)$$

For the CMF8<sub>ladder</sub> spin-1 system on the MnTe lattice, the values of the critical exponents are  $\nu_{\pm} = 0.23$ , and  $B_+/B_- = 0.32$ .

The correlation function plot reveals intriguing features in its dependence on distance, particularly notable at around 7 and 10 Å. These distinctive increments align with directional shifts that correspond to the dominant interaction in the system,  $J_1$ . Significantly, these enhancements in correlation occur when measuring along the direction of  $J_1$ , underscoring the influence of this interaction on the system's correlation behavior. As expected, the correlation length plot demonstrates a divergence near the critical temperature. Furthermore, it is worth noting that the correlation length exhibits a difference before and after this critical point. Specifically, prior to reaching the critical temperature, the correlation length is relatively greater, indicative of the presence of long-range order. In contrast, after passing the critical temperature, there is a reduction in correlation length, suggesting a transition to reduced order or short-range order in the system.

In the context of AFM materials like MnTe, our results are applied to examine the spin correlation functions. MnTe, a spin-5/2 system with a magnetic lattice structure similar to Fig. 1(a), shows the estimated spin correlation functions between different sites in the CMF theory, as illustrated in Fig. 3(b). The substantial AFM interactions in MnTe likely account for the observed specific heat behavior (Fig. 5), and they are anticipated to have a significant impact on the PED thermopower. Notably, a recent study with neutron-scattering measurements also highlights the presence of remnant AFM correlations at high temperatures [16]. Furthermore, it is evident that the larger correlations between the interlayer nearest neighbors in the spin-5/2 system can extend into the disordered phase [Fig. 3(b), green curve].

In magnetic materials, the magnetic specific heat can arise from spin-based entropy carriers such as magnons, spin fluctuations, and Schottky contributions, in addition to nonmagnetic specific heat contributions from phonons, electrons, and dilation [5,6,22,28,43]. In MnTe, the dominant contribution to the magnetic specific heat stems mainly from magnons, exhibiting a distinct behavior with a sharp peak at  $T_N \approx 307$  K and a gradual decrement up to  $\sim 600$  K, contrary to the typical sharp drop observed in many magnetic materials (Fig. 5) [5,6,22,28]. In Fig. 5, we observe the temperature dependence

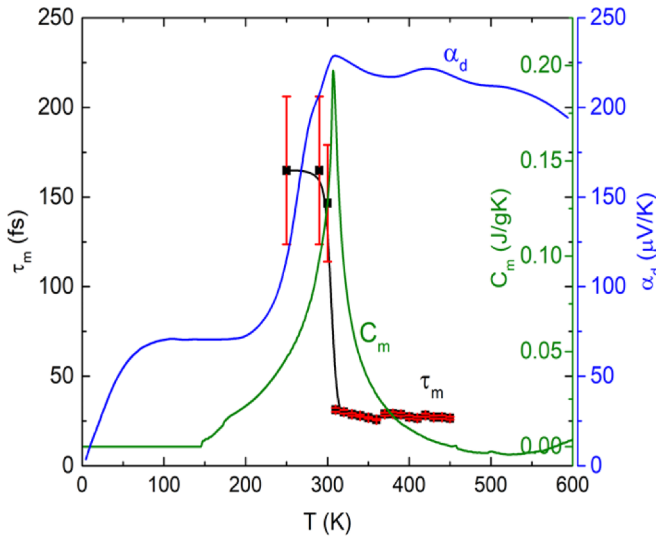


FIG. 5. Experimental evidence of the existence of paramagnons in MnTe: magnon/paramagnon lifetime ( $\tau_m$ ) with the error bar from inelastic neutron scattering, magnetic specific heat ( $C_m$ ) extracted from experimental specific heat, and drag thermopower ( $\alpha_d$ ) calculated by subtracting the electronic contribution from the total thermopower ( $\alpha$ ).

of the drag thermopower, which reveals intriguing insights. Notably, there is a sharp increase in drag thermopower near the critical temperature. Even after crossing the critical temperature threshold, the drag thermopower maintains elevated levels. This behavior strongly suggests the influence of magnons in this temperature range. Additionally, the sustained high values of drag thermopower above the critical temperature provide compelling evidence for the presence of paramagnons. Furthermore, considering the magnon lifetime in the paramagnetic domain as depicted in Fig. 5 adds to the solid experimental support for the PED theory.

Considering the similarities between the spin-1 and spin-5/2 systems, we expect the specific heat trend in the spin-5/2 system to be analogous to that observed in the spin-1 system (Fig. 2), which corroborates with the experimental data of MnTe. This suggests the potential significance of paramagnons in contributing to the thermoelectric properties in the disordered phase and supports the existence of the PED thermopower.

With computational limitations in simulating large clusters for the spin-5/2 system, we acknowledge that the specific heat estimation for MnTe is yet to be fully explored. However, based on the trend observed in the specific heat behavior of the spin-1 system (Fig. 2), it is reasonable to anticipate similar trends in the specific heat for the spin-5/2 system, providing valuable insights into the thermodynamic properties and the role of paramagnons in enhancing thermoelectric performance.

#### IV. DISCUSSION AND SUMMARY

The magnitude of the correlation function between spins decreases as the distance between them increases. Notably, near the critical temperature (e.g.,  $\sim 70$  K for the spin-1

system of Fig. 2), the correlation function is larger compared to temperatures further away from the critical temperature. The fluctuating absolute value of the correlation function is attributed to changes in the exchange interaction type within the cluster as the distance increases. As expected, the correlation length rises, forming a cusp near the critical temperature. In the case of a FM system, this cusp leads to a divergence. However, for an AFM interaction, the peak magnitude remains finite. These observations indicate that the most significant correlations and spin fluctuations occur at the critical temperature.

The temperature dependence of the specific heat is a valuable characteristic that aids in the analysis of experimental data. This behavior can also be derived for a two-spin system at high temperatures by employing a high-temperature expansion method, which reveals a  $T^{-2}$  dependency in the specific heat. This power-law behavior is not limited to specific spin values but holds true for various spin systems. Comparing the specific heat data of spin-5/2 and spin-1 systems demonstrates that the ratio  $C_{5/2}/C_1$  is approximately 20,<sup>1</sup> suggesting that this ratio remains consistent at high temperatures. Thus, the specific heat of the spin-1 system can serve as an estimate for that of the spin-5/2 system in the paramagnetic domain, providing valuable insights for the analysis of experimental data.

In this context, investigating whether paramagnons exhibit quasiparticle behavior with a power-law specific heat as a function of temperature is intriguing. As quantized spin-wave packets arising from thermal fluctuations, paramagnons are expected to contribute significantly to the specific heat due to their association with spin correlations. The persistence of paramagnons at high temperatures suggests quasi-particle-like behavior, leading to the discussed power-law trend in specific heat. Understanding the nature of paramagnons and their connection to the observed power-law behavior requires further theoretical analyses, offering insights into the system's dynamics and the role of short-range order in determining thermodynamic properties.

By considering correlations among spins within clusters that possess a sufficient spin-spin correlation length, we can attribute the paramagnon specific heat to these collective excitations. Notably, when there is a significant disparity in the magnetic interactions between nearest neighbors, the spin-spin correlation becomes more pronounced along the direction of the dominant magnetic interaction above the transition temperature. These enhanced correlations give rise to a nonzero paramagnon specific heat, which in turn supports the observation of the PED thermopower in the disordered phase.

In conclusion, the application of CMF theories has significantly advanced our understanding of correlation functions, correlation lengths, and magnetic properties in various systems. Through our investigation of the contributions of different paramagnon types, which represent collective excitations within distinct clusters, to the specific heat, we have

<sup>1</sup>For a two-spin system, the high-temperature specific heat can be approximately fit by the functional form  $C = 1.25S^{3.3}$ , where  $S$  represents the spin value.

gained profound insights into the thermodynamic behavior of anisotropic magnetic systems. Notably, our findings emphasize the pivotal role of interlayer spin correlations in shaping the heat capacity above critical temperatures, illuminating the intricate interplay between cluster size, spin-spin correlation length, and magnetic interactions. These insights underscore the significance of short-range correlations in elucidating the thermodynamic properties of magnetic materials. The application of CMF theories has proven indispensable in comprehending these complex relationships, offering a com-

prehensive perspective on the underlying physics that govern anisotropic magnetic systems.

## ACKNOWLEDGMENTS

We acknowledge Mohammad Alidoosti for his assistance in running the codes on the supercomputer. This study is partially based upon work supported by the National Science Foundation (NSF) under Grant No. CBET-2110603.

## APPENDIX

### 1. Hamiltonian formulation within CMF theory

In this section, we present the CMF Hamiltonian, employing the CMF theory with clusters containing six and eight sites. Specifically, for the case of a cluster with six sites, the Hamiltonian, denoted as CMF6, is articulated in Eq. (3), where

$$H_c = H_{c-6} = J_1 (\vec{S}_0 \cdot \vec{S}_3 + \vec{S}_1 \cdot \vec{S}_4 + \vec{S}_2 \cdot \vec{S}_5) + J_2 \{ \vec{S}_0 \cdot \vec{S}_1 + \vec{S}_0 \cdot \vec{S}_2 + \vec{S}_1 \cdot \vec{S}_2 + \vec{S}_3 \cdot \vec{S}_4 + \vec{S}_3 \cdot \vec{S}_5 + \vec{S}_4 \cdot \vec{S}_5 \} \\ + J_3 \{ \vec{S}_0 \cdot \vec{S}_4 + \vec{S}_0 \cdot \vec{S}_5 + \vec{S}_1 \cdot \vec{S}_3 + \vec{S}_1 \cdot \vec{S}_5 + \vec{S}_2 \cdot \vec{S}_3 + \vec{S}_2 \cdot \vec{S}_4 \} \quad (\text{A1})$$

$$h_{\text{eff}} = h_{\text{eff}-6} = J_1 \{ \vec{S}_0 \cdot \vec{m}_3 + \vec{S}_1 \cdot \vec{m}_4 + \vec{S}_2 \cdot \vec{m}_5 + \vec{S}_3 \cdot \vec{m}_0 + \vec{S}_4 \cdot \vec{m}_1 + \vec{S}_5 \cdot \vec{m}_2 \} \\ + 2J_2 \{ \vec{S}_0 \cdot (\vec{m}_1 + \vec{m}_2) + \vec{S}_1 \cdot (\vec{m}_0 + \vec{m}_2) + \vec{S}_2 \cdot (\vec{m}_0 + \vec{m}_1) \} \\ + 2J_2 \{ \vec{S}_3 \cdot (\vec{m}_4 + \vec{m}_5) + \vec{S}_4 \cdot (\vec{m}_3 + \vec{m}_5) + \vec{S}_5 \cdot (\vec{m}_3 + \vec{m}_4) \} \\ + 5J_3 \{ \vec{S}_0 \cdot (\vec{m}_4 + \vec{m}_5) + \vec{S}_1 \cdot (\vec{m}_3 + \vec{m}_5) + \vec{S}_2 \cdot (\vec{m}_3 + \vec{m}_4) \} \\ + 5J_3 \{ \vec{S}_3 \cdot (\vec{m}_1 + \vec{m}_2) + \vec{S}_4 \cdot (\vec{m}_0 + \vec{m}_2) + \vec{S}_5 \cdot (\vec{m}_0 + \vec{m}_1) \}, \quad (\text{A2})$$

where six-site clusters are illustrated in Fig. 1(d). Here,  $\vec{m}_i$  is the magnetization vector at the  $i$ th sublattice. For eight-site clusters [see Fig. 1(e)], the different terms of the CMF8 Hamiltonian are given by

$$H_{c-8} = J_1 (\vec{S}_0 \cdot \vec{S}_4 + \vec{S}_1 \cdot \vec{S}_5 + \vec{S}_2 \cdot \vec{S}_6 + \vec{S}_3 \cdot \vec{S}_7) + J_2 \{ \vec{S}_0 \cdot \vec{S}_1 + \vec{S}_0 \cdot \vec{S}_3 + \vec{S}_1 \cdot \vec{S}_2 + \vec{S}_1 \cdot \vec{S}_3 + \vec{S}_2 \cdot \vec{S}_3 \} \\ + J_2 \{ \vec{S}_4 \cdot \vec{S}_5 + \vec{S}_4 \cdot \vec{S}_7 + \vec{S}_5 \cdot \vec{S}_6 + \vec{S}_5 \cdot \vec{S}_7 + \vec{S}_6 \cdot \vec{S}_7 \} + J_3 \left\{ \begin{array}{l} \vec{S}_0 \cdot \vec{S}_5 + \vec{S}_0 \cdot \vec{S}_7 + \vec{S}_1 \cdot \vec{S}_4 + \vec{S}_1 \cdot \vec{S}_6 \\ + \vec{S}_2 \cdot \vec{S}_5 + \vec{S}_2 \cdot \vec{S}_7 + \vec{S}_3 \cdot \vec{S}_4 + \vec{S}_3 \cdot \vec{S}_6 \end{array} \right\} \quad (\text{A3})$$

$$h_{\text{eff}-8} = J_1 \left\{ \begin{array}{l} \vec{S}_0 \cdot \vec{m}_4 + \vec{S}_1 \cdot \vec{m}_5 + \vec{S}_2 \cdot \vec{m}_6 + \vec{S}_3 \cdot \vec{m}_7 \\ + \vec{S}_4 \cdot \vec{m}_0 + \vec{S}_5 \cdot \vec{m}_1 + \vec{S}_6 \cdot \vec{m}_2 + \vec{S}_7 \cdot \vec{m}_3 \end{array} \right\} + J_2 \left\{ \begin{array}{l} \vec{S}_0 \cdot (\vec{m}_1 + 2\vec{m}_2 + \vec{m}_3) + \vec{S}_1 \cdot (\vec{m}_0 + \vec{m}_2 + \vec{m}_3) \\ + \vec{S}_2 \cdot (2\vec{m}_0 + \vec{m}_1 + \vec{m}_3) + \vec{S}_3 \cdot (\vec{m}_0 + \vec{m}_1 + \vec{m}_2) \end{array} \right\} \\ + J_2 \left\{ \begin{array}{l} \vec{S}_4 \cdot (\vec{m}_5 + 2\vec{m}_6 + \vec{m}_7) + \vec{S}_5 \cdot (\vec{m}_4 + \vec{m}_6 + \vec{m}_7) \\ + \vec{S}_6 \cdot (2\vec{m}_4 + \vec{m}_5 + \vec{m}_7) + \vec{S}_7 \cdot (\vec{m}_4 + \vec{m}_5 + \vec{m}_6) \end{array} \right\} + J_3 \left\{ \begin{array}{l} \vec{S}_0 \cdot (3\vec{m}_5 + 4\vec{m}_6 + 3\vec{m}_7) + 3\vec{S}_1 \cdot (\vec{m}_4 + \vec{m}_6 + \vec{m}_7) \\ + \vec{S}_2 \cdot (4\vec{m}_4 + 3\vec{m}_5 + 3\vec{m}_7) + 3\vec{S}_3 \cdot (\vec{m}_4 + \vec{m}_5 + \vec{m}_6) \end{array} \right\} \\ + J_3 \left\{ \begin{array}{l} \vec{S}_4 \cdot (3\vec{m}_1 + 4\vec{m}_2 + 3\vec{m}_3) + 3\vec{S}_5 \cdot (\vec{m}_0 + \vec{m}_2 + \vec{m}_3) \\ + \vec{S}_6 \cdot (4\vec{m}_0 + 3\vec{m}_1 + 3\vec{m}_3) + 3\vec{S}_7 \cdot (\vec{m}_0 + \vec{m}_1 + \vec{m}_2) \end{array} \right\}. \quad (\text{A4})$$

### 2. The definition of a type of clustering approach

Considering that the AFM nearest-neighbor interaction,  $J_1$ , is a prominent factor in our spin model, employing clusters oriented along this direction is likely to yield more accurate results. By partitioning the MnTe lattice into clusters of eight sites along the  $J_1$  direction [as depicted in Fig. 3(b), inset], the Hamiltonians  $H_c$  and  $h_{\text{eff}}$  can be expressed as follows:

$$H_{c-8 \text{ ladder}} = J_1 \{ \vec{S}_0 \cdot \vec{S}_2 + \vec{S}_1 \cdot \vec{S}_3 + \vec{S}_2 \cdot \vec{S}_4 + \vec{S}_3 \cdot \vec{S}_5 + \vec{S}_4 \cdot \vec{S}_6 + \vec{S}_5 \cdot \vec{S}_7 \} + J_2 \{ \vec{S}_0 \cdot \vec{S}_1 + \vec{S}_2 \cdot \vec{S}_3 + \vec{S}_4 \cdot \vec{S}_5 + \vec{S}_6 \cdot \vec{S}_7 \} \\ + J_3 \{ \vec{S}_0 \cdot \vec{S}_3 + \vec{S}_1 \cdot \vec{S}_2 + \vec{S}_2 \cdot \vec{S}_5 + \vec{S}_3 \cdot \vec{S}_4 + \vec{S}_4 \cdot \vec{S}_7 + \vec{S}_5 \cdot \vec{S}_6 \}, \quad (\text{A5})$$

$$\begin{aligned}
h_{\text{eff}}^{\text{8ladder}} &= J_1 (\vec{S}_0 \cdot \vec{m}_6 + \vec{S}_1 \cdot \vec{m}_7 + \vec{S}_6 \cdot \vec{m}_0 + \vec{S}_7 \cdot \vec{m}_1) \\
&+ J_2 \left\{ \begin{array}{l} \vec{S}_0 \cdot (2\vec{m}_0 + 3\vec{m}_1) + \vec{S}_1 \cdot (2\vec{m}_1 + 3\vec{m}_0) \\ + \vec{S}_2 \cdot (2\vec{m}_2 + 3\vec{m}_3) + \vec{S}_3 \cdot (2\vec{m}_3 + 3\vec{m}_2) \\ + \vec{S}_4 \cdot (2\vec{m}_4 + 3\vec{m}_5) + \vec{S}_5 \cdot (2\vec{m}_5 + 3\vec{m}_4) \\ + \vec{S}_6 \cdot (2\vec{m}_6 + 3\vec{m}_7) + \vec{S}_7 \cdot (2\vec{m}_7 + 3\vec{m}_6) \end{array} \right\} \\
&+ J_3 \left\{ \begin{array}{l} \vec{S}_0 \cdot (2\vec{m}_2 + 3\vec{m}_3 + 2\vec{m}_6 + 4\vec{m}_7) \\ + \vec{S}_1 \cdot (2\vec{m}_3 + 3\vec{m}_2 + 2\vec{m}_7 + 4\vec{m}_6) \\ + \vec{S}_2 \cdot (2\vec{m}_0 + 3\vec{m}_1 + 2\vec{m}_4 + 3\vec{m}_5) \\ + \vec{S}_3 \cdot (2\vec{m}_1 + 3\vec{m}_0 + 2\vec{m}_5 + 3\vec{m}_4) \\ + \vec{S}_4 \cdot (2\vec{m}_2 + 3\vec{m}_3 + 2\vec{m}_6 + 3\vec{m}_7) \\ + \vec{S}_5 \cdot (2\vec{m}_3 + 3\vec{m}_2 + 2\vec{m}_7 + 3\vec{m}_6) \\ + \vec{S}_6 \cdot (2\vec{m}_4 + 3\vec{m}_5 + 2\vec{m}_0 + 4\vec{m}_1) \\ + \vec{S}_7 \cdot (2\vec{m}_5 + 3\vec{m}_4 + 2\vec{m}_1 + 4\vec{m}_0) \end{array} \right\}. \quad (\text{A6})
\end{aligned}$$

### 3. Staggered magnetization

In the MnTe system, the preeminent interlayer AFM interaction results in the establishment of a robust staggered magnetization in the ground state, as depicted in Fig. 6 at zero temperature. As the temperature increases, this staggered magnetization gradually diminishes until it completely disappears at the Néel temperature. At this critical point, a phase transition unfolds, marking the shift from the Néel phase to a paramagnetic phase.

Both the MF and CMF theories capture this behavior in their predictions. However, it is important to note that the transition temperature projected by the CMF approach is lower than that obtained through the MF method. This discrepancy

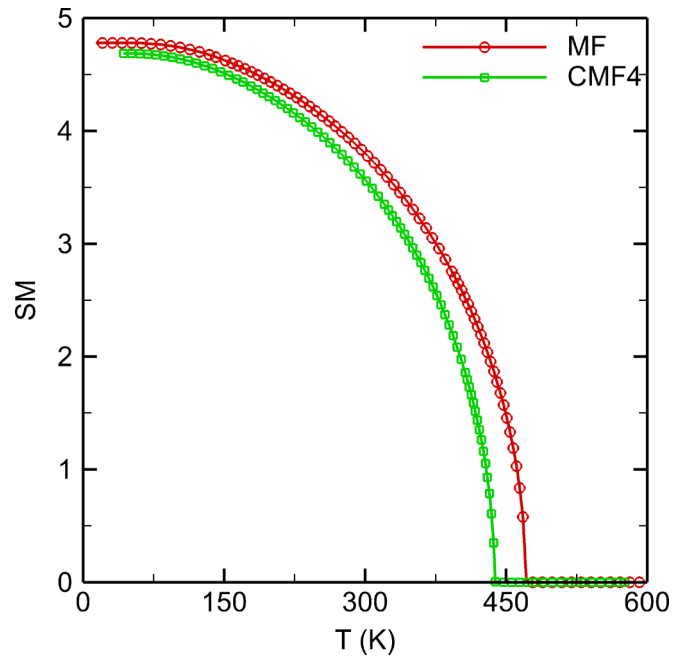


FIG. 6. MF and CMF4 staggered magnetization for the MnTe system.

in transition temperature arises from the incorporation of fluctuations in the CMF method, which are not fully considered in the MF method. These fluctuations introduced by the CMF theory play a role in more accurate estimation of the transition temperature.

- [1] J. He and T. M. Tritt, *Science* **357**, eaak9997 (2017).
- [2] S. T. Goennenwein and G. E. Bauer, *Nat. Nanotechnol.* **7**, 145 (2012).
- [3] M. Y. Kim, S. J. Park, G.-Y. Kim, S.-Y. Choi, and H. Jin, *Energy Environ. Sci.* **14**, 3480 (2021).
- [4] G. E. Bauer, E. Saitoh, and B. J. Van Wees, *Nat. Mater.* **11**, 391 (2012).
- [5] M. M. H. Polash, D. Moseley, J. Zhang, R. P. Hermann, and D. Vashaee, *Cell Rep. Phys. Sci.* **2**, 100614 (2021).
- [6] Y. Zheng, T. Lu, Md M. H. Polash, M. Rasoulianboroujeni, N. Liu, M. E. Manley, Y. Deng, P. J. Sun, X. L. Chen, and H. Zhao, *Sci. Adv.* **5**, eaat9461 (2019).
- [7] M. M. H. Polash, F. Mohaddes, M. Rasoulianboroujeni, and D. Vashaee, *J. Mater. Chem. C* **8**, 4049 (2020).
- [8] B. W. Lebert, B. Bacq-Labreuil, M. P. M. Dean, K. Ruotsalainen, A. Nicolaou, S. Huotari, I. Yamada, H. Yamamoto, M. Azuma, N. B. Brookes *et al.*, *Phys. Rev. B* **108**, 024506 (2023).
- [9] H. Gretarsson, N. H. Sung, J. Porras, J. Bertinshaw, C. Dietl, J. A. N. Bruin, A. F. Bangura, Y. K. Kim, R. Dinnebier, J. Kim *et al.*, *Phys. Rev. Lett.* **117**, 107001 (2016).
- [10] E. da Silva Neto, M. Minola, B. Yu, W. Tabis, M. Bluschke, D. Unruh, H. Suzuki, Y. Li, G. Yu, D. Betto *et al.*, *Phys. Rev. B* **98**, 161114(R) (2018).
- [11] M. Dean, G. Della, R. S. Springell, F. Yakhou-Harris, K. Kummer, N. B. Brookes, X. Liu, Y.-J. Sun, J. Strle, T. Schmitt *et al.*, *Nat. Mater.* **12**, 1019 (2013).
- [12] M. Lucassen, C. Wong, R. Duine, and Y. Tserkovnyak, *Appl. Phys. Lett.* **99**, 262506 (2011).
- [13] B. Wiendlocha, S. Kim, Y. Lee, B. He, G. Lehr, M. G. Kanatzidis, D. T. Morelli, and J. P. Heremans, *Phys. Chem. Chem. Phys.* **19**, 9606 (2017).
- [14] S. M. Wu, J. E. Pearson, and A. Bhattacharya, *Phys. Rev. Lett.* **114**, 186602 (2015).
- [15] W. Zhao, Z. Liu, Z. Sun, Q. Zhang, P. Wei, X. Mu, H. Zhou, C. Li, S. Ma, D. He *et al.*, *Nature (London)* **549**, 247 (2017).
- [16] R. Baral, J. A. Christensen, P. K. Hamilton, F. Ye, K. Chesnel, T. D. Sparks, R. Ward, J. Yan, M. A. McGuire, M. E. Manley *et al.*, *Matter* **5**, 1853 (2022).
- [17] P. Sun, K. R. Kumar, M. Lyu, Z. Wang, J. Xiang, and W. Zhang, *Innovation* **2**, 100101 (2021).
- [18] H. B. Callen, *Thermodynamics and an Introduction to Thermostatistics* (Wiley, New York, 1960).
- [19] C. Goupil, W. Seifert, K. Zabrocki, E. Müller, and G. J. Snyder, *Entropy* **13**, 1481 (2011).
- [20] A. Cracknell and A. Tooke, *Contemp. Phys.* **20**, 55 (1979).
- [21] Md. Mobarak Hossain Polash and D. Vashaee, *Phys. Rev. B* **102**, 045202 (2020).

- [22] M. M. H. Polash, M. Rasoulianboroujeni, and D. Vashaee, *Appl. Phys. Lett.* **117**, 043903 (2020).
- [23] M. Hillert and M. Jarl, *Calphad* **2**, 227 (1978).
- [24] W. Brinkman and S. Engelsberg, *Phys. Rev.* **169**, 417 (1968).
- [25] J. Bauer, A. Hirsch, L. Bayarjargal, L. Peters, G. Roth, and B. Winkler, *Chem. Phys. Lett.* **654**, 97 (2016).
- [26] R. Zimmermann and E. König, *J. Phys. Chem. Solids* **38**, 779 (1977).
- [27] M. M. H. Polash and D. Vashaee, *Phys. Status Solidi RRL* **15**, 2100231 (2021).
- [28] M. M. H. Polash and D. Vashaee, *iScience* **24**, 103356 (2021).
- [29] S. Stølen, F. Grønvold, H. Brinks, T. Atake, and H. Mori, *Phys. Rev. B* **55**, 14103 (1997).
- [30] C. A. Marianetti, K. Haule, G. Kotliar, and M. J. Fluss, *Phys. Rev. Lett.* **101**, 056403 (2008).
- [31] J. Wasscher and C. Haas, *Phys. Lett.* **8**, 302 (1964).
- [32] W. Szuszkiewicz, E. Dynowska, B. Witkowska, and B. Hennion, *Phys. Rev. B* **73**, 104403 (2006).
- [33] R. K. Pathria, *Statistical Mechanics* (Elsevier, New York, 2016).
- [34] L. Onsager, *Phys. Rev.* **65**, 117 (1944).
- [35] T. Oguchi, *Prog. Theor. Phys.* **13**, 148 (1955).
- [36] D. Yamamoto, *Phys. Rev. B* **79**, 144427 (2009).
- [37] D. Yamamoto, A. Masaki, and I. Danshita, *Phys. Rev. B* **86**, 054516 (2012).
- [38] F. Heydarinasab and J. Abouie, *J. Phys.: Condens. Matter* **32**, 165804 (2020).
- [39] F. Heydarinasab and J. Abouie, *Sci. Rep.* **8**, 7955 (2018).
- [40] F. Heydarinasab and J. Abouie, *Phys. Rev. B* **96**, 104406 (2017).
- [41] J. Van Kranendonk and J. Van Vleck, *Rev. Mod. Phys.* **30**, 1 (1958).
- [42] M. Kardar, *Statistical Physics of Fields* (Cambridge University Press, Cambridge, UK, 2007).
- [43] F. Grønvold, N. J. Kveseth, F. D. S. Marques, and J. Tichy, *J. Chem. Thermodyn.* **4**, 795 (1972).